High-Intensity Kapitza-Dirac Effect

P. H. Bucksbaum, D. W. Schumacher, and M. Bashkansky[a]
AT&T Bell Laboratories, Murray Hill, New Jersey 07974
(Received 26 May 1988)

Low-energy (<20 eV) free electrons produced in above-threshold ionization have been scattered by an intense optical standing wave (the Kapitza-Dirac effect). At intensities of 10^{13} to 10^{14} W/cm^2 there is very high momentum transfer between the standing-wave "lattice" and the electrons ($\Delta p \approx 1000\hbar k$). In this regime, the scattering rate approaches the optical frequency, and the electron motion is most easily analyzed by classical mechanics.

PACS numbers: 42.50.Vk

The Kapitza-Dirac (KD) effect is the scattering of a particle beam from a periodic lattice of light. The particles absorb integer multiples of momentum $\hbar\mathbf{G}=2\hbar\mathbf{k}$, where $\mathbf{k}$ is the optical wave vector.[1] For electrons, the KD effect is a form of stimulated Thomson scattering, in which virtual photoabsorption from one of the two traveling-wave modes in the standing wave is accompanied by stimulated emission into the opposing mode [see Fig. 1(a)]. Here we report on the KD effect for electrons in very high-intensity light, where the momentum imparted to the electrons by the light exceeds $\hbar|\mathbf{G}|$ by a factor of 500 or more. The large momentum transfer can be understood in terms of the classical motion of the electron in a spatially periodic effective potential.

The steady-state rate Γ for KD scattering by a nonrelativistic electron in a standing wave produced by two counterpropagating lasers, is given in perturbation theory by

$$\Gamma = n\rho \frac{\partial\sigma_T}{\partial\Omega}\bigg|_{\theta=\pi} = \frac{U_0^2}{\hbar^2\Delta\nu}, \tag{1}$$

where n is the number of photons per mode in the standing wave, ρ is the photon flux from either laser beam, and $\partial\sigma_T/\partial\Omega$ is the differential Thomson cross section, evaluated in the backscattering direction. The right-hand side equality relates Γ to the classical pondermotive potential U_0 of each laser beam[2]

$$U_0 = \frac{e^2 I}{2\pi m_e c \nu^2}, \tag{2}$$

where I is the intensity of each beam, ν its frequency, and $\Delta\nu$ its bandwidth. This is identical to Kapitza and Dirac's original result,[1] except for an enhancement factor of 2 due to polarization (they assumed that the light in the standing wave was unpolarized).

Simultaneous conservation of energy and momentum for electron-photon backscattering leads to a condition

$$a = \lambda\cos\theta, \tag{3}$$

relating the electron de Broglie wavelength a, the optical wavelength λ, and the electron scattering angle θ with respect to $\mathbf{k}$.

These formulae hold for low intensity, but when Γ exceeds the bandwidth of the light, then the relevant coherence time is no longer $1/\Delta\nu$, but the time since the last scattering. For example, for counterpropagating Nd-doped yttrium aluminum garnet laser pulses ($\nu = 2.8\times10^{14}$ Hz) of 100-ps duration ($\Delta\nu \approx 5$ GHz), Γ approaches $\Delta\nu$ for $I \approx 30$ MW/cm^2. This suggests the substitution $\Delta\nu \rightarrow \Gamma$, leading to a modified rate formula:

$$\Gamma = \frac{U_0}{\hbar} = 160\left(\frac{I}{1\,\mathrm{GW/cm^2}}\right)\mathrm{GHz} \tag{4}$$

$$(I > 30\ \mathrm{MW/cm^2}).$$

More modifications are necessary at still higher intensities. The electron mean free path approaches a single wavelength for $I \approx 10$ GW/cm^2, so that the single-scattering momentum-conservation condition [Eq. (3)] no longer holds; at 10^{13} W/cm^2, Γ exceeds the laser frequency! In addition to the lowest-order process in Fig. 1(a), higher-order diagrams leading to the same net momentum transfer [e.g., Fig. 1(b)] become significant, and scattering into higher momentum orders [Fig. 1(c)] and multiple scattering [Fig. 1(d)] also must be taken into account. There have been several attempts to deal with the theory for high intensities.[3-7] Here we present

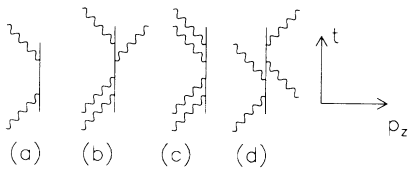

FIG. 1. Feynman graphs for KD scattering. (a) Lowest-order diagram, for net momentum transfer of $+2\hbar\mathbf{k}$. (b) Higher-order corrections to the lowest momentum-transfer peak in (a). (c) Lowest-order diagram for scattering into the next order ($\Delta\mathbf{p}=4\hbar\mathbf{k}$) peak (d) Multiple scattering; in the case shown, there is no *net* momentum transfer.

the first experimental study of the high-intensity KD effect, carried out in standing waves with peak intensities of 10^{13} to 10^{14} W/cm.[2] Previous experiments have all dealt with the lower-intensity regime, where Eqs. (1) and (3) should be valid.[8]

The high-intensity standing waves in this experiment are made by collision of two focused (15-μm waist) laser pulses, derived from a common 100-ps 60-mJ mode-locked amplified Nd-doped yttrium aluminum garnet laser pulse. The spatial mode is an Airy central spot, and the temporal mode is nearly Fourier-transform limited. This is absolutely essential, in order to insure a uniform stationary standing wave during the transit of the electrons through the focus. The intensity, polarization, and arrival time of each beam may be adjusted independently.

The scattered electrons come from above-threshold ionization (ATI) of low-density (10^{8}–10^{10} cm^{-3}) xenon or krypton *in the standing wave itself.*[9] This unconventional source is employed for two reasons: First, ATI electrons are emitted in a narrow distribution in the polarization plane,[9] so that scattering in the $\pm\mathbf{k}$ direction may be observed easily. In addition, the highly nonlinear intensity dependence of ATI (at least eleven photons are required to ionize xenon, twelve for krypton) insures that the electrons have maximum spatial and temporal overlap with the high-intensity standing wave.

The ATI electron energies range from 0 to 20 eV. After scattering out of the focused standing wave, electrons pass through a series of energy-selecting retarding grids, and then impinge on an image-intensified detection screen [Fig. 2(a)] subtending 0.08 sr (66° opening angle). The arrival angles of each electron are recorded. Data collected over many laser pulses are binned to form two-dimensional histograms in θ (the polar angle with respect to $\mathbf{k}$) and ϕ (the azimuthal angle).

Figure 2(b) is a histogram of a typical ATI photoelectron angular distribution from a *single* focused laser beam (no standing wave).[9] Most of the photoelectrons are emitted along the polarization direction. The elongation in azimuthal (ϕ) angles is due to pondermotive scattering from intensity gradients as the electrons leave the focus.[10]

Figure 2(c) shows electrons emitted from a standing wave with the same geometry and polarization as the traveling-wave focus in Fig. 2(b). The angular distribution splits to form two peaks symmetric with respect to the polarization plane. This is the KD effect. It is, however, quite unlike the single-photon scattering case in magnitude; for these electrons have absorbed on the order of 1000 $\hbar k$ of momentum.

We have investigated the dependence of the scattering angle on electron energy, laser polarization, and on the contrast of the standing wave. Most interesting is the

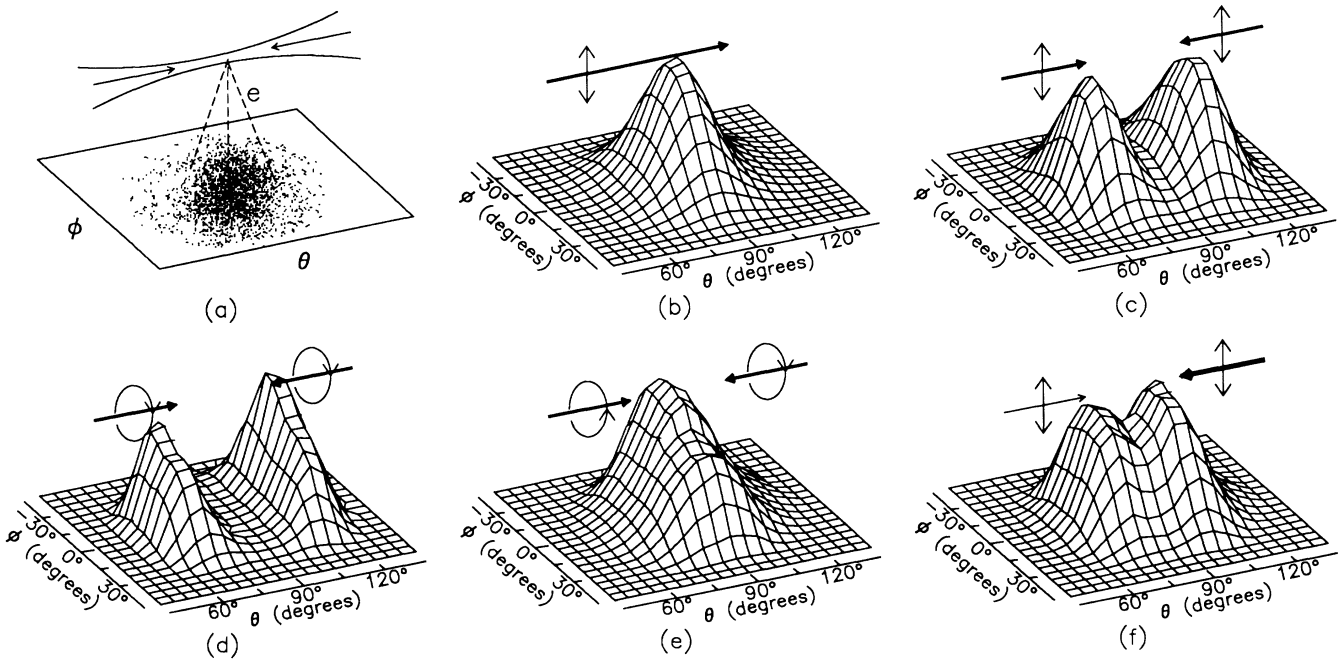

FIG. 2. (a) Experimental geometry. Photoelectrons produced in a standing wave scatter out of the focus, and are detected on a screen. (b)–(f) Electron angular distributions, for electrons that reach the detector with 9 to 12 eV of energy. (b) Typical distribution from xenon ATI in a single 1064-nm laser beam. The peak laser intensity is approximately 8×10^{13} W/cm^2. (c) KD effect in a linearly polarized standing wave. (d) KD effect in a circularly polarized standing wave, with opposite helicities in the two beams. (e) KD effect is absent in a circularly polarized standing wave with equal helicities in the beams. (f) Reduced-contrast standing wave, made from beams of unequal intensities.

effect for a circularly polarized standing wave, shown in Figs. 2(d) and 2(e). If the two light pulses have the opposite helicity (hence equal angular momentum), then KD scattering is quite pronounced [Fig. 2(d)]. If the beams have equal helicity, hence the opposite angular momentum, then stimulated backscattering is forbidden by angular momentum conservation. No KD scattering is expected, or observed [Fig. 2(e)].

Figure 3 shows the θ scattering distribution as a function of electron energy. Lower-energy electrons are scattered at larger angles, but the net momentum transfer is roughly independent of electron energy. Momentum transfer is reduced for a lower-contrast standing wave, however, as shown in Fig. 2(f).

At these high intensities, nonperturbative methods that treat the light as a time-varying potential are more useful than perturbation theories.[6,7] In the nonrelativistic plane-wave approximation, Schrödinger's equation may be written

$$\frac{[\mathbf{P}-(e/c)\mathbf{A}(\mathbf{x},t)]^2}{2m_e}\Psi(\mathbf{x},t)=i\hbar\frac{\partial\Phi(\mathbf{x},t)}{\partial t}, \tag{5}$$

where $\mathbf{A}(\mathbf{x},t)$ is the classical (nonquantized) time-dependent vector potential for a standing wave produced by two counterpropagating plane waves along $\hat{\mathbf{z}}$

$$\mathbf{A}(\mathbf{x},t)=A_0[\hat{\epsilon}_1\cos(kz+\omega t)+\hat{\epsilon}_2\cos(kz+\omega t)]. \tag{6}$$

Following Ref. 6, we resort to a classical approximation, where the Hamiltonian operator on the left-hand side of Eq. (5) becomes a classical Hamiltonian H describing the motion of a nonrelativistic spinless electron in a standing light wave.

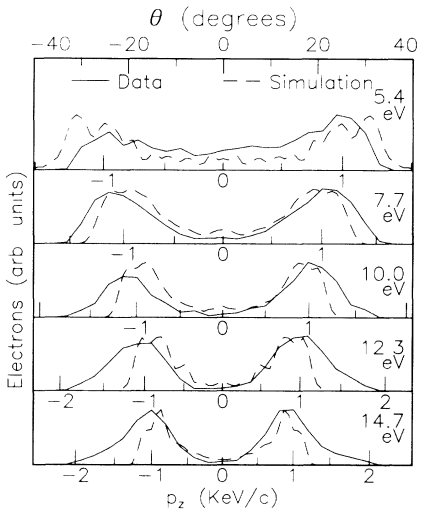

FIG. 3. Polar-angle distributions for electrons of different energies in the same standing wave. All distributions are plotted vs polar angle (top scale). Bottom scale: the momentum transfer for each energy. Solid lines are data, collected in a 2-eV window bracketing the energy shown. Dashed lines are results of Monte Carlo electron trajectories.

For slowly moving electrons, the rapidly oscillating portion of H may be replaced by a time-averaged spatially periodic effective potential. If $\hat{\epsilon}_1$ and $\hat{\epsilon}_2$ are identical linear polarizations, then the effective potential takes the form $U_p(z)=4U_0\cos^2(kz)$. Thus the KD effect is simply scattering from a periodic potential of height $4U_0$. Equation (4) must be replaced by a position-dependent scattering rate

$$\Gamma_{1\to 2}(z)=\frac{2U_0}{\hbar}\sin(2kz), \tag{7}$$

where $1\to 2$ means that this is the *net* scattering rate of photons from beam 1 to beam 2. This rate can be positive or negative. Quantum calculations in the high-intensity limit yield similar results [Ref. 7, Eqs. (46)-(49)].

This classical Hamiltonian is identical to that of a simple pendulum of mass m_e and length $1/(2k)$ under a uniform force $4kU_0$.[11] Electrons whose total energy E is less than the antinodal maximum potential $4U_0$ are localized in a sinusoidal potential well centered on an electric-field node of the standing wave, where they oscillate with angular frequency

$$\Omega=\omega\frac{\pi}{\chi(E)}\left(\frac{2U_0}{m_ec^2}\right)^{1/2}. \tag{8}$$

Here $\chi(E)$ is a complete elliptic integral of the first kind

$$\chi(E)=\int_0^{\pi/2}\frac{dx}{[1-(E/4U_0)^2\sin^2x]^{1/2}}. \tag{9}$$

For example, the oscillation period for a 1-eV electron in a peak potential of 10 eV (corresponding to $\approx 10^{14}$ W/cm^2 for Nd-doped yttrium aluminum garnet radiation) is 0.3 ps.

In order to compare our results with the predictions of this classical approximation, we have calculated electron trajectories with a time-varying spatially periodic pondermotive potential appropriate for a standing wave formed by two perfectly overlapped 100-ps pulses meet-

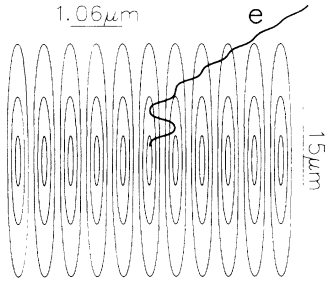

FIG. 4. The calculated trajectory of an ATI electron drifting out of the standing wave, showing one cycle of bound motion in a potential trough, followed by a transition from bound to unbound motion along $\hat{\mathbf{z}}$.

ing in a TEM_{00} Gaussian focus. Electrons were launched in a simulation according to a very simple model, in which all ionization takes place at a single threshold intensity. Atoms are therefore only ionized near the antinodes. They are initially directed along the laser polarization, but immediately begin to oscillate in the $\pm\mathbf{k}$ direction under the influence of the pondermotive spatial grating. Eventually they migrate to the edges of the beam, where the standing-wave intensity is lower. At some point, after several oscillations, the electrons reach a part of the focus with a low enough potential to convert from bound to unbound motion. This is shown for a single trajectory in Fig. 4. Histograms for Monte Carlo generated electron distributions at several energies are shown in Fig. 3. Results employing an ionization intensity of 3×10^{13} W/cm^2 are quite consistent with the data.[10] The larger momentum transfer observed for electrons leaving a circularly polarized standing wave [Fig. 2(d)] appears in the simulations to be the result of a higher ionization threshold intensity for ATI with circular polarization.

We have demonstrated the Kapitza-Dirac effect at light intensities where the scattering rate equals or exceeds the optical frequency. The results resemble classical scattering of point electrons from a pondermotive grating. This pondermotive approach is expected to break down at still higher intensities, when the oscillation frequency of an electron bound in the standing-wave potential well approaches an optical cycle. This regime also corresponds to the onset of relativistic effects in the electron motion. Intensities of this magnitude will be available in the near future.

We wish to acknowledge useful discussions with R. R. Freeman and with R. Jensen.

---

[a]Previous affiliation: Columbia University, New York, NY 10027. Present address: Naval Research Laboratory, Washington, DC 20375.

[1]P. L. Kapitza and P. A. M. Dirac, Proc. Cambridge Philos. Soc. **29**, 297 (1933).

[2]L. S. Brown and T. W. B. Kibble, Phys. Rev. **133**, A705 (1965); P. H. Bucksbaum, M. Bashkansky, and T. J. McIlrath, Phys. Rev. Lett. **58**, 349 (1987).

[3]E. A. Coutsias and J. K. McIver, Phys. Rev. A **31**, 3155 (1985).

[4]R. Gush and H. P. Gush, Phys. Rev. D **3**, 1912 (1971).

[5]L. S. Bartell, J. Appl. Phys. **38**, 1561 (1967).

[6]Y. W. Chan and W. L. Tsui, Phys. Rev. A **20**, 294 (1979).

[7]M. V. Fedorov, Zk. Eksp. Teor. Fiz. **52**, 1434 (1967) [Sov. Phys. JETP **25**, 952 (1967)].

[8]Attempts to observe the KD effect for electrons at low intensities include L. S. Bartell, R. R. Roskos, and H. B. Thompson, Phys. Rev. **166**, 1494 (1968); H. Schwarz, Phys. Lett. **43A**, 457 (1973); Y. Takeda and I. Matsui, J. Phys. Soc. Jpn. **25**, 1202 (1968); H. C. Pfeiffer, Phys. Lett. **26A**, 326 (1968). The KD effect in atoms has been studied by P. J. Martin, B. G. Oldaker, A. H. Miklich, and D. E. Pritchard, Phys. Rev. Lett. **61**, 515 (1988); and P. L. Gould, G. A. Ruff, and D. E. Pritchard, Phys. Rev. Lett. **56**, 827 (1986).

[9]T. J. McIlrath, P. H. Bucksbaum, R. R. Freeman, and M. Bashkansky, Phys. Rev. A **35**, 4611 (1987).

[10]R. R. Freeman, T. J. McIlrath, P. H. Bucksbaum, and M. Bashkansky, Phys. Rev. Lett. **57**, 3156 (1986).

[11]See any standard mechanics text, for example, A. Sommerfeld, *Mechanics* (Academic, New York, 1952), pp. 87–90.